An Adaptive Artificial Potential Function Approach for Geometric Sensing

Guoxian Zhang and Silvia Ferrari

Abstract— **In this paper, a novel artificial potential function is proposed for planning the path of a robotic sensor in a partially observed environment containing multiple obstacles and multiple targets. The sensor planning problem considered in this paper consists of planning the motion of a robot with an on-board sensor that is deployed in order to support a sensing objective, such as, target detection and classification, by gathering sensor measurements over time. An adaptive potential function approach is presented such that the sensor path accounts for prior information on the target geometry and information profit, by traveling a minimum distance.**

I. INTRODUCTION

Sensor path planning is concerned with planning the measurements of a sensor in order to support sensing objectives, such as target detection, classification and localization. When the sensor's field-of-view (FOV) or visibility region is bounded, the sensor's position and orientation determine what targets can be measured at any given time. Therefore, the sensor path must be planned in concert with the measurement sequence. When sensors are installed on robotic platforms and are deployed in an obstacle-populated environment, the sensor path must also avoid collisions between the platform and the obstacles or other robots [1]–[3]. The problem of planning the sensor path in order to maximize the information profit, while minimizing the distance traveled and avoiding collisions with the obstacles, is referred to as treasure hunt [4]–[6]. This problem is relevant to many sensor applications such as, robotic mine hunting [7], cleaning [1], and robotic games [8], as well as the monitoring of urban environments [9], manufacturing plants [10], and endangered species [11]. Cell decomposition [4], [5] and probabilistic roadmap methods [12] have been successfully developed for solving geometric sensor path planning problems, such as the treasure hunt, when a prior model of the obstacles and the targets is available. In this paper, a novel potential function approach is presented for generating sensor paths that can be utilized on-line, i.e., when obstacles and targets are not all known *a priori*, but are sensed during the motion.

Although effective methods, such as potential field, have been developed for robot motion planning, they are not directly applicable to geometric sensor path planning because they do not take into account the geometries of the targets and of the sensor FOV, and do not consider the information value of the sensor measurements [13]–[19]. In the classical potential field method [20]–[23], for example, the robot's objective is to navigate the workspace to reach a goal configuration by following the negative gradient of a potential function that is designed to provide a repulsive potential near the obstacles and an attractive potential toward the goal configuration. Although the potential field method is well suited to on-line motion planning and to convergence analysis, its effectiveness is limited by the tendency of the robot to get stuck in local minima of the potential function [24]. An effective approach for escaping local minima is to follow a new local path generated through a random-walk algorithm.

In this paper, a novel potential function is presented for generating attractive potentials toward the targets, based on their geometries and information value. Then, a novel algorithm for escaping local minima is developed based on the probabilistic roadmap method (PRM). PRM is a sampling method where a set of robot configurations, referred to as milestones, are sampled from a probability density function defined based on the robot's and obstacles' geometries. Subsequently, using a query-and-search algorithm, a graph or roadmap is constructed that provides an efficient one-dimensional representation of the geometry of the free configuration space. Finally, robot paths between an initial and final configuration are obtained by searching the roadmap for the shortest path using a search algorithm [25]. PRM is one of the most efficient and effective path planning algorithms for planning robot paths off line. Recently, the authors developed an information roadmap method inspired by PRM, but applicable to geometric sensor path planning [12], [26]. This method generates a roadmap by sampling a probability density function defined based on the sensor's FOV, and on targets' geometries and information value modeled from prior information, such as geophysical maps and prior sensor measurements.

One of the key results presented in this paper is that the same adaptive potential function can be used to generate the navigation potential and the information roadmap, thereby providing a natural framework for integrating the two approaches. A method is presented for using the adaptive information roadmap to escape local minima of the potential function in place of random-walk algorithms that can lead the sensor to regions of poor information value. In a cooperative sensor network, the adaptive information roadmap can also be exchanged between robots and used to plan the path of other robots based on the latest sensed information. By defining a potential function in configuration space, the approach accounts for the geometries and positions of the obstacles, targets, sensor's platform and FOV. The information value of the targets is represented by defining the potential function in terms of their expected mutual information or entropy reduction conditioned on prior sensor measurements. As a

result, the sensor visits targets that offer the best tradeoff between distance and information value, and when extended to on-line sensor path planning, it can adapt its path based on new sensor measurements obtained from targets or obstacles that were previously undetected.

II. PROBLEM FORMULATION AND ASSUMPTIONS

This paper addresses the problem of planning the path of a robotic sensor with a platform geometry $\mathcal{A} \subset \mathbb{R}^2$, and a FOV geometry $\mathcal{S} \subset \mathbb{R}^2$, that navigates a workspace $\mathcal{W} \subset \mathbb{R}^2$ for the purpose of making measurements from multiple targets in a partially observed environment. For simplicity, in this paper $\mathcal{A}$ and $\mathcal{S}$ are assumed to be convex polygons. Since the sensor is installed on-board the robotic platform, $\mathcal{S}$ can be assumed to have a fixed position and orientation with respect to $\mathcal{A}$. The robotic sensor workspace $\mathcal{W}$ is populated with n fixed obstacles $B = \{\mathcal{B}_1, \ldots, \mathcal{B}_n\} \subset \mathcal{W}$ and m fixed targets $T = \{\mathcal{T}_1, \ldots, \mathcal{T}_m\} \subset \mathcal{W}$ with $\mathcal{B}_i \cap \mathcal{T}_j = \emptyset$ for $\forall i \in I_B$ and $\forall j \in I_T$, where I_B and I_T are the index sets of B and T. Prior information, such as airborne sensor measurements and environmental maps, is used to estimate the geometry and location of obstacles and targets in B and T (as shown in [27]).

In standard estimation theory, a sensor that obtains a vector of measurements $\mathbf{Z} \in \mathcal{Z} \subset \mathbb{R}^r$ in order to estimate an unknown state vector $\mathbf{x} \in \mathcal{X} \subset \mathbb{R}^n$ is modeled as,

$$\mathbf{Z}^k = \mathbf{h}(\mathbf{x}^k, \boldsymbol{\lambda}^k) \tag{1}$$

where $\mathbf{h} : \mathbb{R}^n \times \mathbb{R}^\wp \to \mathbb{R}^r$ is a deterministic vector function that is possibly nonlinear, $\boldsymbol{\lambda} \in \mathbb{R}^\wp$ is the random vector representing the sensor characteristics, such as sensor mode, environmental conditions, and sensor noise or measurement errors. It is assumed that the sensor model is time invariant and k is the discrete time index. In many sensor applications, however, the state, the measurements, and the sensor characteristics also are random vectors. Therefore, a more general observation or measurement model that has been adopted in the literature is the joint probability mass function (PMF) $p(\mathbf{Z}^k, \mathbf{X}^k, \boldsymbol{\lambda}^k)$. This joint PMF may be given by the factorization,

$$p(\mathbf{Z}^k, \mathbf{X}^k, \boldsymbol{\lambda}^k) = p(\mathbf{Z}^k \mid \mathbf{X}^k, \boldsymbol{\lambda}^k) p(\mathbf{X}^k) p(\boldsymbol{\lambda}^k) \tag{2}$$

which includes the conditional PMF $p(\mathbf{Z}^k \mid \mathbf{X}^k, \boldsymbol{\lambda}^k)$, the priors $p(\mathbf{X}^k)$ and $p(\boldsymbol{\lambda}^k)$, and assumes that $\mathbf{X}^k$ and $\boldsymbol{\lambda}^k$ are independent. Various sensors, including infrared, ground penetrating radars, and synthetic aperture radars have been modeled as (2) in target detection, classification, and tracking applications [28]–[32]. In this paper, the joint PMF in (2) is considered to be the sensor model, and is assumed known. Since the sensor model holds for all targets and environmental conditions, and can be assumed to remain constant over time, (2) can be written as $p(\mathbf{Z}_i, \mathbf{X}_i, \boldsymbol{\lambda}_i)$ for every target $\mathcal{T}_i \in T$.

The purpose for deploying the robotic sensor in $\mathcal{W}$ is to obtain measurements from a subset of targets in T. To each target $\mathcal{T}_i \in T$, there is associated an information value denoted by V_i that is computed by the information function defined in Section IV, and represents the expected benefit of making measurements from $\mathcal{T}_i$, based on the sensor model and on prior information. V_i can be considered as the expected uncertainty reduction for target features or classification. Let $\mathcal{F}_\mathcal{A}$ be a moving Cartesian frame embedded in $\mathcal{A}$. Then, every point of $\mathcal{A}$ and every point of $\mathcal{S}$ have a fixed position with respect to $\mathcal{F}_\mathcal{A}$, and the configuration $\mathbf{q} = (x\ y\ \theta) \in SE(2)$ is used to specify the position (x, y) and orientation θ of both $\mathcal{A}$ and $\mathcal{S}$ with respect to a fixed inertial frame $\mathcal{F}_\mathcal{W}$, embedded in $\mathcal{W}$. Obstacles and targets are also assumed to be fixed and rigid in $\mathcal{W}$, such that every point of $\mathcal{B}_i$, for $\forall i \in I_B$, and every point of $\mathcal{T}_j$, $\forall j \in I_T$, have a fixed position with respect to $\mathcal{F}_\mathcal{W}$. Let $\mathcal{C}$ denote the space of all possible robot configurations. Then, the path of the robotic platform's centroid is defined as a continuous map $\tau : [0, 1] \to \mathcal{C}$, with $\mathbf{q}_0 = \tau(0)$ and $\mathbf{q}_f = \tau(1)$, where $\mathbf{q}_0$ and $\mathbf{q}_f$ are the initial and final configurations, respectively. Since $\mathcal{S}$ is mounted on $\mathcal{A}$, the path τ determines the targets in $\mathcal{W}$ that can be measured by the robotic sensor, while traveling from $\mathbf{q}_0$ to $\mathbf{q}_f$.

While the platform $\mathcal{A}$ must avoid collisions with the obstacles B, the sensor's FOV $\mathcal{S}$ must intersect $\mathcal{T}_i$ in order to obtain the measurements $\mathbf{Z}_i$. Since $\mathcal{S}$ is mounted on $\mathcal{A}$, the platform motion must be planned in concert with the sensor measurements, and the path τ must simultaneously avoid obstacles while searching for targets. Let the measurement set of a robotic sensor along a path τ be defined as $Z(\tau) = \{\mathbf{Z}_i \mid \mathcal{T}_i \cap \mathcal{S}(\mathbf{q}) \neq \emptyset,\ \tau(s) = \mathbf{q},\ s \in [0, 1],\ i \in I_T\}$, where $\mathcal{S}(\mathbf{q})$ is the subset of $\mathcal{W}$ occupied by $\mathcal{S}$ at a configuration $\mathbf{q}$, along τ. Then, the robotic sensor path τ between $\mathbf{q}_0$ and $\mathbf{q}_f$ must avoid all obstacles in $\mathcal{W}$, and maximize the information value of the measurement set $Z(\tau)$ by traveling the minimum distance.

III. BACKGROUND ON POTENTIAL FIELD

The potential field method is a robot motion planning technique that utilizes an artificial potential function to find the obstacle-free path of shortest distance in an Euclidian workspace. The obstacles and the goal configuration, are considered as sources to construct a potential function U which represents the characteristics of the configuration space. Although different approaches have been utilized to generate U [21]–[23], the potential function always consists of two components, the attractive potential U_{att} generated by the goal configuration, and the repulsive potential U_{rep}, generated by the obstacles. The total potential is given by,

$$U(\mathbf{q}) = U_{att}(\mathbf{q}) + U_{rep}(\mathbf{q}) \tag{3}$$

where $\mathbf{q}$ is any configuration in $\mathcal{C}$. The force applied on the robot is proportional to the negative gradient of U,

$$\nabla U(\mathbf{q}) = [\frac{\partial U(\mathbf{q})}{\partial q_1}, \frac{\partial U(\mathbf{q})}{\partial q_2}, \ldots, \frac{\partial U(\mathbf{q})}{\partial q_n}]^T \tag{4}$$

where $\mathbf{q} = [q_1, q_2, \ldots, q_n]^T \in \mathbb{R}^n$.

A C-obstacle is defined as the subset of $\mathcal{C}$ that causes collisions with at least one obstacle in B, i.e., $\mathcal{CB}_i \equiv \{\mathbf{q} \in$

$\mathcal{C} \mid \mathcal{A}(\mathbf{q}) \cap \mathcal{B}_i \neq \emptyset\}$, where $\mathcal{A}(\mathbf{q})$ denotes the subset of $\mathcal{W}$ occupied by the platform geometry $\mathcal{A}$ when the robot is at the configuration $\mathbf{q}$. The union of all C-obstacles obtained from B is referred to as the C-obstacle region. Thus, in searching for targets in $\mathcal{W}$, the robotic sensor is free to rotate and translate in the free configuration space, which is defined as the complement of the C-obstacle region $\mathcal{CB}$ in $\mathcal{C}$, i.e., $\mathcal{C}_{free} = \mathcal{C} \backslash \mathcal{CB}$ [20].

As shown in [20], the repulsive potential can be represented as,

$$U_{rep}(\mathbf{q}) = \begin{cases} \frac{1}{2}\eta(\frac{1}{\rho(\mathbf{q})} - \frac{1}{\rho_0})^2 & \text{if} \quad \rho(\mathbf{q}) \leq \rho_0 \\ 0 & \text{if} \quad \rho(\mathbf{q}) > \rho_0 \end{cases} \tag{5}$$

where η is a scaling factor, $\rho(\mathbf{q})$ is the distance between the robot and the nearest obstacle in Euclidean space, and ρ_0 is a constant parameter that is chosen by the user. The attractive potential is given by,

$$U_{att}(\mathbf{q}) = \frac{1}{2}\varepsilon\rho^2_{goal}(\mathbf{q}) \tag{6}$$

where ε is a scaling factor, and $\rho_{goal}(\mathbf{q})$ is the distance between the robot and the goal configuration. In (5) and (6), only the obstacle closest to $\mathbf{q}$ is considered to generate $U_{rep}(\mathbf{q})$, and the target is assumed to be a single point in $\mathcal{C}_{free}$. This makes the potential function difficult to update when new obstacles and targets are sensed during the path execution, because for each value of $\mathbf{q}$, the potential needs to update by computing its distance from the closest obstacle and target.

In the following section, a novel potential function is presented that takes into account the geometries of the sensor's FOV and of the targets, as well as the information value estimated from the sensor model (2).

IV. ADAPTIVE POTENTIAL FIELD METHOD FOR GEOMETRIC SENSOR PATH PLANNING

A. Artificial Potential Function for Geometric Sensing

The potential function proposed in this paper is additive with respect to obstacles and targets, i.e.,

$$U(\mathbf{q}) = \sum_{i=1}^{m} U_i(\mathbf{q})_{rep} + \sum_{i=1}^{n} U_i(\mathbf{q})_{att} \tag{7}$$

where $U_i(\mathbf{q})_{rep}$ is the repulsive potential generated by the ith obstacle, $U_i(\mathbf{q})_{att}$ is the attractive potential generated by the ith target, m is the number of obstacles, and n is the number of targets that are yet to be measured. By defining the potential function as shown in (7), it is easy to remove the potential of a target after it is measured by the sensor and to add the potential of a new detected obstacle on-line. $U_i(\mathbf{q})_{rep}$ is similarly defined as,

$$U_i(\mathbf{q})_{rep} = \begin{cases} \frac{1}{2}\eta_1(\frac{1}{\rho^b_i(\mathbf{q})} - \frac{1}{\rho_0})^2 & \text{if} \quad \rho^b_i(\mathbf{q}) \leq \rho_0 \\ 0 & \text{if} \quad \rho^b_i(\mathbf{q}) > \rho_0 \end{cases} \tag{8}$$

where η_1 is a scaling parameter showing the influence of obstacles, ρ_0 is the influence distance of obstacles, and $\rho^b_i(\mathbf{q})$ is the distance between $\mathbf{q}$ and the ith obstacle.

Since the target geometries are considered, $\rho^t_i(\mathbf{q})$, which is the distance between $\mathcal{T}_i$ and $\mathbf{q}$, needs to be first computed to generate $U_i(\mathbf{q})_{att}$. The C-target defined as,

$$\mathcal{CT}_i = \{\mathbf{q} \in \mathcal{C} | \mathcal{T}_i \cap \mathcal{S}(\mathbf{q}) \neq \emptyset\} \tag{9}$$

is utilized to describe the set of $\mathbf{q}$ in $\mathcal{C}_{free}$ for which the robotic sensor can measure $\mathcal{T}_i$, as proposed by the authors in previous work [5], [12]. The distance $\rho^t_i(\mathbf{q})$ is computed as,

$$\rho^t_i(\mathbf{q}) = \min_{\mathbf{q}_i \in \mathcal{CT}_i} ||W \cdot (\mathbf{q}_i - \mathbf{q})|| \tag{10}$$

where $||\cdot||$ represents the Euclidian norm, and W is a diagonal and positive definite matrix representing the importance of changes in position and orientation.

The information value of each target $\mathcal{T}_i$ can be measured by various information metrics based on prior information. One way is to use mutual information which is based on shannon entropy. The uncertainty of the hidden variable for $\mathcal{T}_i$, denoted by $\mathbf{X_i}$, given the prior information $\mathbf{e}$, can be represented by the conditional entropy

$$H(\mathbf{X_i}|\mathbf{e}) = \sum_{\mathbf{x_i}} P(\mathbf{x_i}|\mathbf{e}) log P(\mathbf{x_i}|\mathbf{e}) \tag{11}$$

Hence, the expected decrease of uncertainty of $\mathbf{X}_i$ by a posterior measurement $\mathbf{Z^k_i}$ can be measured by the mutual information

$$\begin{aligned} I(\mathbf{X_i}; \mathbf{Z^k_i}|\mathbf{e}) &= H(\mathbf{X_i}|\mathbf{e}) - EH(\mathbf{X_i}|\mathbf{Z^k_i}, \mathbf{e}) \\ &= H(\mathbf{X_i}|e) - \sum_{\mathbf{z^k_i}} P(\mathbf{z^k_i}|\mathbf{e}) H(\mathbf{X_i}|\mathbf{z^k_i}, \mathbf{e}) \end{aligned} \tag{12}$$

In this paper, the information value V_i of the target $\mathcal{T}_i$, estimated by $I(\mathbf{X_i}; \mathbf{Z^k_i}|\mathbf{e})$ in (12), is used to construct the potential function, such that the sensor path takes into account the expected benefit of making measurement from $\mathcal{T}_i$ prior to visiting the target. The attractive potential function has the following properties.

1) $U_i(\mathbf{q})_{att}$ is an increasing function of the distance $\rho^t_i(\mathbf{q})$. When $\rho^t_i(\mathbf{q})$ goes to infinity, the potentials generated by different targets are the same.
2) At a configuration $\mathbf{q}$ having the same distance to two targets, the target with a higher information value has a lower potential value and a higher gradient at $\mathbf{q}$.
3) The potential generated by the target with the higher information value has the bigger distance of influence.

To achieve these objectives, we propose an attractive function for the ith target that is defined as,

$$U_i(\mathbf{q})_{att} = \eta_2(1 - \sigma V^a_i e^{-\frac{\rho^t_i(\mathbf{q})^2}{2\sigma V^a_i}}) \tag{13}$$

where η_2 is a scaling parameter representing the influence of targets, V_i is the information value of the ith target, and σ is the influence parameter which together with V_i and parameter a decides the influence diameter of the ith target. It can be shown that (13) satisfies the above properties. Let $\rho_i = \rho^t_i(\mathbf{q})$, $U_i(\rho_i)_{att}$ can also be regarded as a function of

ρ_i. The first order derivative of $U_i(\rho_i)_{att}$ is,

$$g(\rho_i) = \frac{dU_i(\rho_i)_{att}}{d\rho_i} = \eta_2 \rho_i e^{-\frac{\rho_i^2}{2\sigma V_i^a}} \tag{14}$$

g is positive for all $\rho_i > 0$, which shows that $U_i(\rho)_{att}$ is an increasing function of ρ_i. Also from (13),

$$\lim_{\rho_i \to \infty} U_i(\rho_i)_{att} = \eta_2 \tag{15}$$

so property 1) is satisfied. For any given $\mathbf{q}$ and any positive parameter a, $\sigma V_i^a e^{-\frac{\rho_i^t(\mathbf{q})^2}{2\sigma V_i^a}}$ is an increasing function of V_i. Then $U_i(\mathbf{q})_{att}$ is a decreasing function of V_i. Since η_2 and ρ_i are both nonnegative, (14) shows that for given ρ_i, the first derivative of $U_i(\rho_i)_{att}$ is an increasing function of V_i, and hence property 2) is satisfied. At last, to demonstrate property 3), we use the inflection point of $U_i(\rho_i)_{att}$ as the influence distance of the ith target. The second derivative of $U_i(\rho_i)_{att}$ is as shown in (16),

$$\frac{dg(\rho_i)}{d\rho_i} = \eta_2 (1 - \frac{\rho_i^2}{\sigma V_i^a}) e^{-\frac{\rho_i^2}{2\sigma V_i^a}} \tag{16}$$

(16) is a decreasing equation of ρ_i and setting it to zero will give us the influence distance of the ith target $\rho_i = \sqrt{\sigma V_i^a}$. Then the proposed attractive function can be combined with the repulsive potential to generate the potential field.

B. Local Information Roadmap Adaptation

Various methods have been proposed to overcome the limitations of potential field, in particular to escape the local minima of the potential function. When the workspace dimension is low, such as two or three dimensions, robots can escape a local minimum by filling the well. However, when the workspace dimension is high, this method is no longer feasible due to its computational complexity. Then other methods, usually random methods, are used to help the robots escape the local minima, for instance randomized path planning [20]. In this paper, we utilize the potential function to generate a local information roadmap around a local minimum to navigate the robotic sensor escaping the local minimum and achieving its sensing objective. Different from normal randomized path planning, information roadmap in our method considers the probability of achieving targets after escaping the local minima during milestones sampling. This makes it more applicable in multiple targets problem. Since PRM has also been proved to be applicable for high dimensional workspace, by combining potential field and information roadmap our method will be applicable for high dimensional space in future work.

Suppose the robotic sensor arrives at a local minimum, called $\mathbf{u}_{loc}$. The probability density function for sampling milestones at $\mathbf{q}$ is defined as,

$$f(\mathbf{q}) = \begin{cases} \frac{e^{-U(\mathbf{q})}}{\int_{\mathcal{U}} e^{-U(\mathbf{q})} d\mathbf{q}} & \mathbf{q} \in \mathcal{U} \\ 0 & \mathbf{q} \notin \mathcal{U} \end{cases} \tag{17}$$

where $\mathcal{U} \subset \mathcal{C}$ is a randomly generated subspace around $\mathbf{u}_{loc}$. By defining $f(\mathbf{q})$ as shown in (17), configurations which are close to high value targets and far away from obstacles in $\mathcal{U}$ have high probability to be sampled. Then a specific number of milestones $\{c_1, c_2, \ldots, c_k\}$ can be sampled with *Direct Methods* [33]. Call $\mathbf{u}_{loc}$ as c_0, the set $C = \{c_0, c_1, c_2, \ldots, c_k\}$ together with a local planner which connects milestones with straight lines in $\mathcal{C}_{free}$ is used to construct the roadmap. While the normal roadmap construction method first constructs the roadmap with sampled milestones and then tries to connect the initial configuration into the roadmap, this first put the initial configuration into roadmap and then extend it with the set of sampled milestones. The reason is that in our problem the purpose is to escape the local minimum, so we have to first guarantee $\mathbf{u}_{loc}$ is in this roadmap. After $\mathbf{u}_{loc}$ is included in the roadmap, milestones that can be connected to $\mathbf{u}_{loc}$ are used to help the robotic sensor escape the local minimum. The process of constructing the roadmap is shown in Fig. 1. The roadmap is initialized as $G_0 = c_0$. At the first step, the milestones, which can be connected to $\mathbf{u}_{loc}$ by the local planner, construct the first step roadmap G_1, and the remaining milestones form a set C_1 to construct the roadmap at the next step; then at step i, the milestones in C_{i-1} which can be connected to G_{i-1} are added to form G_i. The process stops when $G_{i-1} = G_i$, and then $G = G_i$. If $G = G_0$ the construction fails and new milestones need to be regenerated to construct the roadmap.

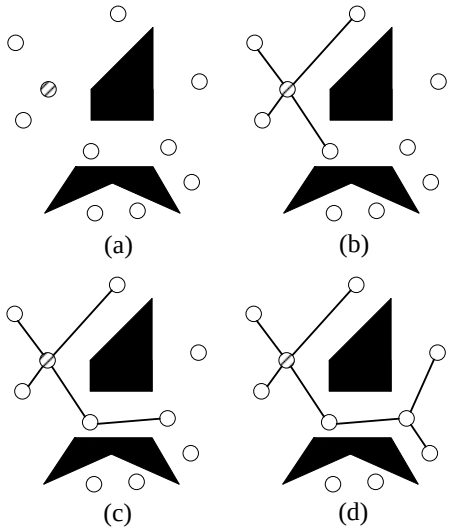

Fig. 1. Process to construct the roadmap: (a) initial milestones; (b) first step; (c) second step; (d) final step. dash circle: local minimum; white circle: milestones; black area: C-obstacles

After the roadmap is constructed, it is utilized to allow the robotic sensor to escape the local minimum by checking whether a milestone in the roadmap can navigate the robotic sensor to a configuration with lower potential. The process is as follows:

Step I: A local information roadmap is constructed based on the local minimum at $\mathbf{u}_{loc}$ where the samples are generated with (17). Let the set $G_{left} = G$.

Step II: If G_{left} is empty, go to step IV; otherwise randomly

choose a milestone $c_i \in G_{left}$ and utilize the best-first motion path planning starting at $\mathbf{u}_{loc}$ to generate a path τ_i and achieve a new local minimum $\mathbf{u}_{loc}^{'}$. Best-first motion is a path planning method in which the path $\{\mathbf{q}_0, \mathbf{q}_1, \ldots, \mathbf{q}_n\}$ is generated by choosing the next configuration $\mathbf{q}_i$ as the neighbor of the configuration $\mathbf{q}_{i-1}$ with the smallest potential value U [20].

Step III: If $\mathbf{u}_{loc}^{'} < \mathbf{u}_{loc}$, τ_i is added to the current path τ, and then go to step V; otherwise, delete c_i from G_{left} and go back to step II.

Step IV: Assume for each c_i in G, its corresponding generated path with step II is τ_i. τ is the path from the initial configuration to the local minimum $\mathbf{u}_{loc}$. Select a backtracking configuration for the robotic sensor path. If τ includes at least one local minimum, then the backtracking configuration is up to a random chosen local minimum in τ; otherwise, it equals the last configuration in τ_i with i randomly chosen. The backtracking configuration is considered as the last configuration of the updated path.

Step V: The robotic sensor successfully escapes the local minimum. The path and current configuration are updated.

In our simulation, we assume that, along the path, the robotic sensor can at most generate m local information roadmaps, where m is chosen by the author. If the robotic sensor fails to measure the desired number of targets with generating no more than m local information roadmaps, the robotic sensor fails to finish the job.

V. ANALYSIS

The purpose of the proposed method is to find a path for a robotic sensor in a partially observed environment. The robotic sensor is assumed to move in the workspace with a constant speed, and the gradient of the potential U is used to determine the path of the robotic sensor. If the potential field is directly used as the input to control the robotic sensor, some changes may be needed. The following dynamical model,

$$M(\mathbf{q})\ddot{\mathbf{q}} + f(\mathbf{q}, \dot{\mathbf{q}}) + g(\mathbf{q}) = \tau \tag{18}$$

can be used to describe the robotic sensor [23], [34]. Where $M(\mathbf{q})$ is the robotic sensor's inertia matrix, $f(\mathbf{q}, \dot{\mathbf{q}})$ is the fictitious force, $g(\mathbf{q})$ is the gravitational force, and τ is the control input. By the feedback control law we have,

$$\tau(\mathbf{q}, \dot{\mathbf{q}}) = -\nabla U(\mathbf{q}) + d(\mathbf{q}, \dot{\mathbf{q}}) \tag{19}$$

where $d(\mathbf{q}, \dot{\mathbf{q}})$ is an arbitrary dissipative force. In order not to obtain an infinite repulsive potential when the robotic sensor approaches the obstacles [23], the potential $U_i(\mathbf{q})_{rep}$ is modified to as,

$$U_i(\mathbf{q})_{rep} = \begin{cases} \frac{1}{2}\eta_1(\frac{1}{\rho_i^b(\mathbf{q})+b} - \frac{1}{\rho_0})^2 & \text{if} \quad \rho_i^b(\mathbf{q}) \leq \rho_0 \\ 0 & \text{if} \quad \rho_i^b(\mathbf{q}) > \rho_0 \end{cases} \tag{20}$$

where b is a small constant.

We assume that no targets are very close to the obstacles, that is when the robotic sensor approaches the targets, the repulsive potential generated by the obstacles is zero. Then, the potential function is given by,

$$U(\mathbf{q}) = \sum_{i=1}^{n} U_i(\mathbf{q})_{att} = \sum_{i=1}^{n} \eta_2(1 - \sigma V_i^a e^{-\frac{\rho_i^t(\mathbf{q})^2}{2\sigma V_i^a}}) \tag{21}$$

By differentiating (21), in most cases $\mathbf{q} \in \mathcal{CT}_i$ is not a local minimum for the potential field. However, by choosing σ much bigger than η_2 we can guarantee that for each $\mathcal{CT}_i$ there will be a set of local minima close to the targets, thereby making them measurable by the robotic sensor. During dynamic control of the sensor, this problem can be solved by utilizing a smaller dissipative input d.

VI. SIMULATIONS AND RESULTS

In this section, simulations are developed to test the method proposed above under the following assumptions. The robotic sensor platform is assumed to be a rectangle; however, its FOV may have different shapes. The workspace is also a rectangle. Obstacle geometries, and target geometries and information values are assumed to be known *a priori*. The purpose of the robotic sensor is to measure a specific number of targets in the workspace to obtain high information values and travel a small distance. The method developed in Section IV is utilized to generate the potential field in the simulated workspace. The configuration space $\mathcal{C}$ is decomposed into square bins and time is discretized into discrete time steps. At each time step, the robotic sensor is assumed to be able to move to its adjacent bins or stay in its current bin. Its direction is determined by the potential function. Results are averaged over 100 trials.

A. Influence of Sensor FOV Geometry

In this subsection, the simulations are used to illustrate how the geometries of the robotic sensor FOV and targets influence the path. The goal of the robotic sensor is to take measurements of two targets in the workspace as shown in Fig. 2. The robotic sensor is assumed only to be able to translate in the workspace. Four targets with different information values are deployed in the field. Some robot configurations along the path are plotted in this figure. As can be seen, the robotic sensor chooses to measure $\mathcal{T}_3$ after measuring $\mathcal{T}_1$, since to measure $\mathcal{T}_2$, which has the second highest information value, it has to move back and travel a long distance. However, when the geometry of $\mathcal{T}_1$ and $\mathcal{S}$ change as in Fig. (3), the robotic sensor is able to measure $\mathcal{T}_1$ and $\mathcal{T}_2$ which have the highest two measurement values with a short travel distance. In this simple example, no undesirable local minimum exists. The results of this example show how the geometries of the targets and sensor FOV may affect the robotic sensor's decision on path planning.

B. Adaptive Information Roadmap Method

In this subsection, we illustrate how the adaptive information roadmap method affects the robotic sensor paths generated by the potential field. As shown in Fig. 4, a robotic sensor is trying to measure one target in this workspace. Starting from the initial configuration, the robotic sensor will navigate to a local minimum. Then a local information

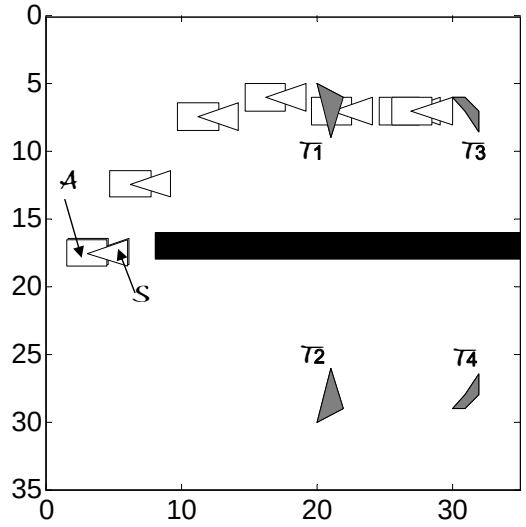

Fig. 2. A path generated by the potential field. black area: obstacle; grey area: targets; information value: $\mathcal{T}_1 = 0.3$, $\mathcal{T}_2 = 0.2$, $\mathcal{T}_3 = 0.1$, $\mathcal{T}_4 = 0.1$

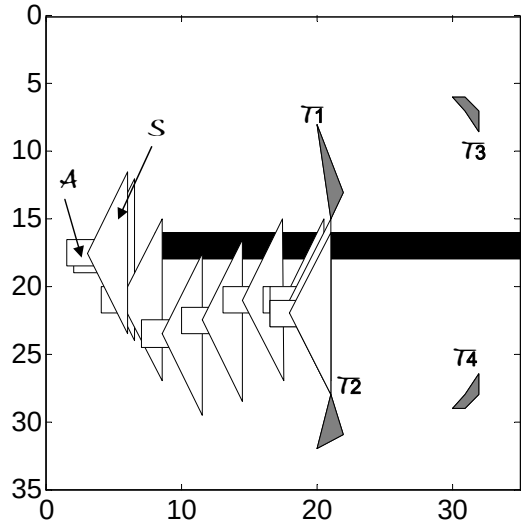

Fig. 3. A path generated by the potential field. black area: obstacle; grey area: targets; information value: $\mathcal{T}_1 = 0.3$, $\mathcal{T}_2 = 0.2$, $\mathcal{T}_3 = 0.1$, $\mathcal{T}_4 = 0.1$

roadmap has to be generated. Fig. 4 shows a generated path by our method. The path generated by the information roadmap is shown as dotted lines. Since the local information roadmap is used in our method, the generated paths are random. Table I shows the results of 100 runs in this workspace. From the results we can see that about 80% of the time, the local information roadmap navigates the robotic sensor to the target with higher information value.

In the third simulation, we consider a more complicated field with twelve targets and ten obstacles. The goal of the robotic sensor is to measure six targets in this field. The robotic sensor is assumed to be able to both translate and rotate freely in the workspace. Among the twelve targets, $\mathcal{T}_1$, $\mathcal{T}_5$, $\mathcal{T}_7$ and $\mathcal{T}_9$ have higher information values than other targets. Two possible geometries of sensor FOV are

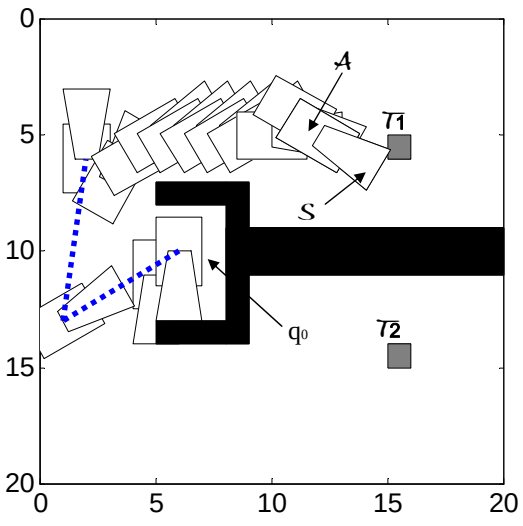

Fig. 4. Local information roadmap effect on the robotic sensor path planning. black area: obstacle; grey area: targets; information value: $\mathcal{T}_1 = 0.3$, $\mathcal{T}_2 = 0.1$

TABLE I

NUMBER OF TARGET MEASUREMENTS IN 100 RUNS ($\sigma = 100$, $\eta_2 = 0.2$, $a = 2$)

Target number i	1	2
Information Value V_i	0.30	0.10
Measurement Times	78	22

considered in this simulation. A searched path under each condition is shown in Fig. 5 and Fig. 6. Table II shows the results of 100 runs in this workspace with each sensor FOV.

From the results we can see high value targets $\mathcal{T}_1$ and $\mathcal{T}_5$ are measured over 90% of the runs under both conditions. For $\mathcal{T}_9$ when the sensor has a large FOV, about 20% of the times the sensor moves to measure $\mathcal{T}_9$ since it does not take a long travel to reach it; however, when the sensor FOV is small, it seems not valuable to measure $\mathcal{T}_9$, because the travel distance is too long and there are few other targets around $\mathcal{T}_9$. Another interesting result is that with a small robotic sensor FOV, $\mathcal{T}_7$ is measured many more times than in the case of the robotic sensor with a large FOV. The reason is that in order to measure the high value $\mathcal{T}_5$, the robotic sensor with a small FOV has to travel across the narrow passage containing $\mathcal{T}_5$. This makes it difficult for the sensor to measure $\mathcal{T}_8$. Then after measuring the high value $\mathcal{T}_1$, the sensor will have one more chance to measure a target and the best choice is the value $\mathcal{T}_7$ just below $\mathcal{T}_1$. The number of measurements of $\mathcal{T}_{12}$ also has an obvious difference between two the robotic sensors. The reason is that with a small FOV, the influence of $\mathcal{T}_4$ and $\mathcal{T}_5$ is small compared to the one of $\mathcal{T}_{12}$ when the robotic sensor is at the initial position. Therefore the robotic sensor chooses to measure $\mathcal{T}_{12}$ first. However, when the FOV is large, the influence of $\mathcal{T}_4$ and $\mathcal{T}_5$ are high and the robotic sensor is more likely to choose

to measure $\mathcal{T}_4$ and $\mathcal{T}_5$. These two examples show both how the geometry of sensor FOV influences the paths and how the local information roadmap leads the robotic sensor to configurations that can be navigated to measure high value targets.

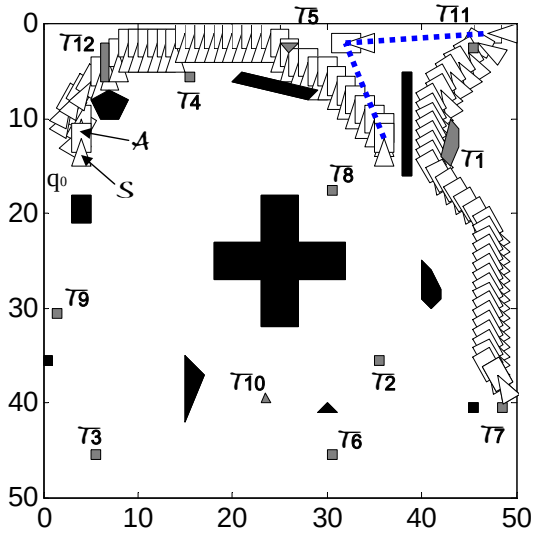

Fig. 5. A workspace with 10 obstacles, 12 targets, and a searched path for small sensor FOV. black area: obstacles; grey area: targets; dotted lines: paths generated by local information roadmap

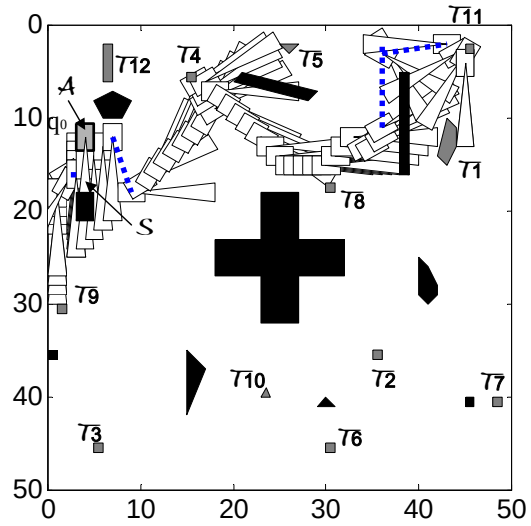

Fig. 6. A workspace with 10 obstacles, 12 targets, and a searched path for large sensor FOV. black area: obstacles; grey area: targets; dotted lines: paths generated by local information roadmap

VII. CONCLUSIONS AND FUTURE WORK

This paper presents a methodology to utilize the information value and geometries of targets and the robotic sensor to construct a potential field for a workspace with multiple targets and obstacles. The potential field includes the trade off between the information value and travel distance for target measurements. The potential function is also used to construct the local information roadmaps to help the robotic sensor escape the local minima. Simulation results show that the proposed potential field can successfully utilize the knowledge of target geometry and information value to improve its path. Targets with high information values that are close to the robotic sensor are more likely to be measured when the measurement number is limited. Future work will focus on the following two aspects. First, high dimensional cases will be studied in measuring multiple targets. Second, the method will be extended to on-line path planning for both single robotic sensor and multiple robotic sensors.

VIII. ACKNOWLEDGMENTS

This work was supported by the National Science Foundation, under grant ECS CAREER 0300236. Thanks Gianluca Di Muro for reading the early drafts of this paper.

REFERENCES

[1] C. Hofner and G. Schmidt, "Path planning and guidance techniques for an autonomous mobile cleaning robot," *Robotics and Autonomous Systems*, vol. 14, pp. 199–212, 1995.

[2] E. U. Acar, "Path planning for robotic demining: Robust sensor-based coverage of unstructured environments and probabilistic methods," *International Journal of Robotic Research*, vol. 22, no. 441-466, 2003.

[3] C. Kreucher, K. Kastella, and A. Hero, "Multi-platform information-based sensor management," *Proc. of SPIE*, vol. 5820, pp. 141–151, 2005.

[4] S. Ferrari and C. Cai, "Information-driven search strategies in the board game of clue," *IEEE Transactions on Systems, Man, and Cybernetics - Part B*, vol. 39, no. 3, pp. 607–625, 2009.

[5] C. Cai and S. Ferrari, "Information-driven sensor path planning by approximate cell decomposition," *IEEE Transactions on Systems, Man, and Cybernetics - Part B*, vol. 39, no. 3, pp. 672–689, 2009.

[6] S. Ferrari, R. Fierro, B. Perteet, C. Cai, and K. Baumgartner, "A geometric optimization approach to detecting and intercepting dynamic targets using a mobile sensor network," *SIAM Journal on Control and Optimization*, vol. 48, no. 1, pp. 292–320, 2009.

[7] R. Siegel, "Land mine detection," *IEEE Instrumentation and Measurement Magazine*, vol. 5, no. 4, pp. 22–28, 2002.

[8] T. Weigel, J. Gutmann, M. Dietl, A. Kleiner, and B. Nebel, "Cs freiburg: Coordinating robots for successful soccer playing," *IEEE Transactions on Robotics and Automation*, vol. 18, no. 5, pp. 685–699, 2002.

[9] S. Ferrari, C. Cai, R. Fierro, and B. Perteet, "A multi-objective optimization approach to detecting and tracking dynamic targets in pursuit-evasion games," in *Proc. of the 2007 American Control Conference*, New York, NY, 2007, pp. 5316–5321.

[10] D. Culler, D. Estrin, and M. Srivastava, "Overview of sensor networks," *Computer*, vol. 37, no. 8, pp. 41–49, 2004.

[11] P. Juang, H. Oki, Y. Wang, M. Martonosi, L. Peh, and D. Rubenstein, "Energy efficient computing for wildlife tracking: Design tradeoffs and early experiences with zebranet," *ACM SIGOPS Operating Systems Review*, vol. 36, pp. 96–107, 2002.

[12] G. Zhang, S. Ferrari, and M. Qian, "Information roadmap method for robotic sensor path planning," *Journal of Intelligent and Robotic Systems*, vol. 56, no. 1-2, pp. 69–98, 2009.

[13] N. Rao, S. Hareti, W. Shi, and S. Iyengar, "Robot navigation in unknown terrains: Introductory survey of non-heuristic algorithms," in *Technical Report ORNL/TM-12410*, Oak Ridge National Laboratory, Oak Ridge, TN, 1993.

[14] N. Rao, "Robot navigation in unknown generalized polygonal terrains using vision sensors," *IEEE Transactions on System, Man, and Cybernetics*, vol. 25, no. 6, pp. 947–962, 1995.

[15] A. Lazanas and J. C. Latombe, "Motion planning with uncertainty - a landmark approach," *Artificial Intelligence*, vol. 76, pp. 287–317, 1995.

[16] K. Song and C. C. Chang, "Reactive navigation in dynamic environment using a multisensor predictor," *IEEE Transactions on Systems, Man, and Cybernetics - Part B*, vol. 29, no. 6, pp. 870–880, 1999.

TABLE II

THE NUMBER OF TARGET MEASUREMENTS IN 100 RUNS ($\sigma = 300$, $\eta_2 = 0.2$, $a = 2$)

Target number i	1	2	3	4	5	6	7	8	9	10	11	12
Information Value V_i	0.30	0.15	0.15	0.15	0.3	0.15	0.3	0.15	0.3	0.15	0.15	0.15
Measurement times with small FOV	100	3	0	100	100	0	95	5	0	0	97	100
Measurement times with large FOV	94	2	6	100	100	0	62	93	21	2	94	26

[17] M. Kazemi, M. Mehrandezh, and K. Gupta, "Sensor-based robot path planning using harmonic function-based probabilistic roadmaps," *Proc. ICAR '05, 12th International Conference on Advanced Robotics*, pp. 84–89, 2005.

[18] Z. Sun and J. Reif, "On robotic optimal path planning in polygonal regions with pseudo-eucledian metrics," *IEEE Transactions on Systems, Man, and Cybernetics - Part A*, vol. 37, no. 4, pp. 925–936, 2007.

[19] X.-C. Lai, S.-S. Ge, and A. Al-Mamun, "Hierarchical incremental path planning and situation-dependent optimized dynamic motion planning considering accelerations," *IEEE Transactions on Systems, Man, and Cybernetics- Part A*, vol. 37, no. 6, pp. 1541–1554, 2007.

[20] J. C. Latombe, *Robot Motion Planning*. Kluwer Academic Publishers, 1991.

[21] J. Ren and K. Mclsaac, "A hybird-systems approach to potential field navigation for a multi-robot team," in *Proc. of IEEE International Conference on Robotics and Automation*, Taipei, Taiwan, 2003, pp. 3875–3880.

[22] S. Shimoda, Y. Kuroda, and K. Iagnemma, "Potential field navigation of high speed unmanned ground vehicles on uneven terrain," in *Proc. of IEEE International Conference on Robotics and Automation*, Barcelona, Spain, 2005, pp. 2839–2844.

[23] S. Ge and Y. Cui, "New potential functions for mobile robot path planning," *IEEE Transactions on Robotics and Automation*, vol. 16, no. 5, pp. 615–620, 2000.

[24] Y. Koren and J. Borenstein, "Potential field methods and their inherent limitations for mobile robot navigation," in *Proc. of IEEE Conference on Robotics and Automation*, Sacramento, CA, 1991, pp. 1398–1404.

[25] L. E. Kavraki, P. Svetska, J. C. Latombe, and M. H. Overmars, "Probabilistic roadmaps for path planning in high-dimensional configuration space," *IEEE Transactions on Robotics and Automation*, vol. 12, no. 4, pp. 566–580, 1996.

[26] M. Qian and S. Ferrari, "Probabilistic deployment for multiple sensor systems," in *Proc. of the 12^{th} SPIE Symposium on Smart Structures and Materials: Sensors and Smart Structures Technologies for Civil, Mechanical, and Aerospace Systems*, vol. 5765, San Diego, 2005, pp. 85–96.

[27] C. Scrapper and A. Takeuchi, "Using a priori data for prediction and pbject recognition in an autonomous mobile vehicle," *Proc. SPIE Unmanned Ground Vehicle Technology*, vol. 5083, pp. 414–418, 2003.

[28] K. Kastella, "Discrimination gain to optimize detection and classification," *IEEE Transactions on Systems, Man, and Cybernetics - Part A*, vol. 27, no. 1, pp. 112–116, 1997.

[29] C. Kreucher, K. Kastella, and A. Hero, "Sensor management using an active sensing approach," *Signal Processing*, vol. 85, pp. 607–624, 2005.

[30] C. Kreucher, A. Hero, and K. Kastella, "A comparison of task driven and information driven sensor management for target tracking," in *Proc. of the IEEE Conference on Decision and Control*, Seville, Spain, 2005, pp. 4004–4009.

[31] S. Ferrari and A. Vaghi, "Demining sensor modeling and feature-level fusion by bayesian networks," *IEEE Sensors*, vol. 6, pp. 471–483, 2006.

[32] C. Cai, S. Ferrari, and Q. Ming, "Bayesian network modeling of acoustic sensor measurements," in *Proc. IEEE Sensors*, Atlanta, GA, 2007, pp. 345–348.

[33] G. Casella and R. Berger, *Satistical Inference*. Duxbury Press, 2001.

[34] E. Rimon and D. Kodischek, "Exact robot navigation using artificial potential functions," *IEEE Transactions on Robotics and Automation*, vol. 8, no. 5, pp. 501–518, 1992.